



Characterization of CBD–CdS nanocrystals doped with Co²⁺

Jorge I. Contreras-Rascón¹ · Joel Díaz-Reyes² · Mariana E. Linares-Avilés³ · Karla N. Rivera-Hernández² · Miguel Galván-Arellano⁴ · José S. Arias-Cerón⁴ · Javier Martínez-Juárez⁵

Received: 12 July 2018 / Accepted: 20 September 2018 / Published online: 24 September 2018
© Springer Science+Business Media, LLC, part of Springer Nature 2018

Abstract

Co-doped CdS nanofilms are synthesised by chemical bath deposition growth technique at the temperature of 60 ± 2 °C. The cobalt molar fraction was ranged from $0 \leq x \leq 5.47$, which was determined by energy-dispersive X-ray spectroscopy. The X-ray diffraction shows that the nanofilms are of CoS–CdS nanocomposites with individual CdS and CoS crystalline planes. The Co-doped CdS crystalline phase was zinc-blende that was determined by X-ray diffraction and confirmed by Raman spectroscopy. The average grain size of the CdS films was ranged from 2.56 to 1.67 nm that was determined by Debye–Scherrer equation from ZB (111) direction and it was confirmed by Wang equation and high resolution transmission electron microscopy (HRTEM). Raman scattering shows that the CdS lattice dynamics is characteristic of a bimodal behaviour, in which the first optical longitudinal mode denotes the characteristic peak at 305 cm^{-1} of the CdS nanocrystals that is associated with the cobalt incorporation. Nanofilms present two main bandgaps at ~ 2.56 and 3.80 eV, which are attributed to single CdS and quantum-confinement due to nanocrystals size. The increase in band gap with increase in cobalt concentration suggests intermetallic compound of CoS ($E_g = 1.60$ eV) with CdS ($E_g = 2.44$ eV). The CdS nanocrystals size was ranged from 2.46 to 1.81 nm that was determined from ZB (111) direction by Debye–Scherrer equation and confirmed by the Wang equation. The room-temperature photoluminescence of the Co-doped CdS presents well-resolved radiative bands associated to structural defects and with the quantum-confinement. For the Co-doped CdS the photoluminescence intensity increases indicate a high-passivation of the nanocrystals.

1 Introduction

Recently several research groups have observed that the incorporation of magnetic ions into crystalline lattices of various materials II–VI allow the possible application to devices based on the spin of free electrons with unprecedented capabilities. Various growth techniques have pointed out the ferromagnetic properties [1–3] and paramagnetic [4, 5] of this type of materials. However, the usefulness of CdS for the futuristic devices resides in the ability to dope it with impurities so as to achieve the desired properties and to make them multifunctional. As innovative as the binary nanostructures of materials II–VI, ZnTe and PbTe, in which the detector can respond to a modeled radiation and also as base materials for solar cells [6]. Transition metal (TM) such as Mn, Fe, Co, Zn, etc., doped with CdS has drawn considerable attention as it offers a great opportunity to integrate electrical, optical and magnetic properties into a single material, which makes it an ideal candidate for nonvolatile memory, magneto-optical and future spintronic devices [7]. Due to quantum confinement effects and

✉ Joel Díaz-Reyes
joel_diaz_reyes@hotmail.com

¹ Universidad Politécnica Metropolitana de Puebla, Ingeniería en Biotecnología, Popocatepetl s/n. Tres Cerritos, Puebla, Puebla 72480, Mexico

² Centro de Investigación en Biotecnología Aplicada, Instituto Politécnico Nacional, Ex-Hacienda de San Juan Molino, Km. 1.5, Tepetitla, Tlaxcala 90700, Mexico

³ Unidad Profesional Interdisciplinaria de Biotecnología, Instituto Politécnico Nacional, Av. Acueducto Poniente, La Laguna Ticomán, Ciudad de México 07340, Mexico

⁴ Depto. de Ingeniería Eléctrica, SEES, CINVESTAV-IPN, Apartado Postal 14-740, Ciudad de México 07000, Mexico

⁵ Centro de Investigaciones en Dispositivos Semiconductores, Benemérita Universidad Autónoma de Puebla, Ciudad Universitaria, Edif. No. 137. Av. 14 Sur y San Claudio. Col. San Manuel, Puebla, Puebla 72570, Mexico

rapid increase in surface-to-volume ratio as particle diameters are reduced to strong confinement regime, optical and magnetic properties are enhanced to large extent [8]. Compounds containing transition metal ions, e.g., $Zn_{1-x}Mn_xSe$, $Zn_{1-x}Co_xSe$, and $Cd_{1-x}Fe_xSe$, are known as diluted magnetic semiconductors. The presence of magnetic ions leads to a number of unusual electronic and optical properties, which are due to the interaction of the magnetic ion with band electrons as well as to the exchange interaction between the magnetic ions themselves [9]. The optical properties of Co^{+2} in II–VI compounds have been studied rather extensively in samples containing cobalt impurities [10]. In recent years, II–VI semiconductors doped with transition-metal ions, such as Cr:ZnSe, Co:ZnSe, Co:ZnS and Co-CdSe have been explored as candidates for saturable-absorber Q-switches used with eye-safe lasers having output near 1.54 μm [11]. Nanostructured transducers of CdS doped with Zn have been synthesised using the thermal evaporation method [12]. In fact semiconductors in which their band gap energy has been stimulated have been reported as heterogeneous photocatalysts such as the Mg-doped ZnO and ZnO/rGO nanocomposites [13].

2 Materials and synthesis of CdS nanofilms

The technique of obtaining Co-doped CdS was the chemical bath deposition [14] in its immersion modality (vapour bath) to prevent pollution, a water bath equipment is used with internal recirculation to control the reaction, which uses a microprocessor that achieves the precision of ± 0.1 °C. Being graded it to the temperature of 60 ± 2 °C to avoid polymorphism obtaining one of the well-defined crystalline phases at low temperatures [15, 16] and to avoid the release of harmful gases into the environment by the use of ammonium nitrate as complexing agent [17]. The solutions mixture is carried out using the following precursors: cadmium chloride dihydrate ($CdCl_2 + 2H_2O$) (Productos Químicos Monterrey S. A.), potassium hydroxide (KOH) (JT Baker, 98.6% purity), Ammonia Nitrate ($NH_4(NO_3)$) (Sigma-Aldrich, 99.5% purity) and thiourea (NH_2SCNH_2) (Fermet, 99.9% purity). The doping reagent is cobalt carbonate(II) ($CoCO_3$) (Carl-Roth 46%) working with the following concentrations 0.05 M $CdCl_2$, 0.05 M KOH, 0.1 M $NH_4(NO_3)$, 0.05 M NH_2SCNH_2 , which are poured into a Pyrex glass beaker. The used substrates are borosilicate glasses of dimensions, 1 in \times 3 in, and thickness ± 1 –2 mm, which are adhered to the walls of the beaker. For undoped CdS was labelled as M1 in Tables and characterizations graphs, M2 and M3 for those doped with cobalt, respectively. The concentrations of the precursors are $CoCO_3$ 0.001 M with the appropriate volumes, the doping is achieved when the solutions mixture has a slightly basic pH, the deposit time is

measured from this moment. Finally, the samples are treated in air for decarboxylation at a temperature higher than that used for the synthesis of the nanofilms.

3 Characterization techniques

The Co-doped CdS nanofilms chemical stoichiometry was obtained by energy dispersive spectrometry (EDS), which was carried out in a System LEO 438VP, with W.D. of 26 mm using a pressure of 20 Pa. The crystalline phase and structure of the films were determined with a Bruker D8 Discover diffractometer using the copper $K\alpha$ radiation ($\lambda = 1.5406$ Å) at 40 kV and 40 mA with parallel beam geometry. Raman scattering was performed using the 632.8 nm line of a He–Ne laser at normal incidence for excitation. The light was focused to a diameter of 6.0 μm at the sample using a 50 \times (numerical aperture 0.9) microscope objective. The nominal laser power used in these measurements was 20 mW. Scattered light was analysed using a micro-Raman system (Lambram model of Dilor), a holographic notch filter made by Kaiser Optical System, Inc. (model superNotch-Plus), a 256 \times 1024-pixel CCD used as detector cooled to 140 K using liquid nitrogen, and two interchangeable gratings (600 and 1800 g/mm). High resolution transmission electron microscopy (HRTEM) studies were carried out in a JEOL JEM200 of 80–200 kv, the obtained image is recorded with a CCD camera in real time. The Gatan Digital Micrograph software was used for the analysis of HRTEM images. The transmittance measurement was performed using a Bruker Infrared Spectrometer Vertex 70 at room temperature. The photoluminescence was measured using a He–Cd (Omnichrome-Series 56) laser emitting at 325 nm with an optical excitation power of ~ 15 mW at room temperature. The radiative emission from the sample was focalized to the entrance slit of a HRD-100 Jobin–Yvon double monochromator with a resolution better than 0.05 nm, and detected with an Ag–Cs–O Hamamatsu photomultiplier with a spectral response in the range 350–1000 nm.

4 Results and discussion

The chemical stoichiometry of the $Cd_{1-x}Co_xS$ nanofilms was estimated by EDS measurements. The information of the elemental composition was generated by keeping the electron beam fixed at several points of the sample, in which the total scan was performed (global analysis), which besides allowed to know the presence of the residual impurities [18, 19]. Figure 1 shows a typical EDS spectrum of sample M1, since each sample was mapped taking 10 $\mu m \times 10 \mu m$ areas. The EDS results presented in Table 1 correspond to the average of them for each sample, which are included the atomic

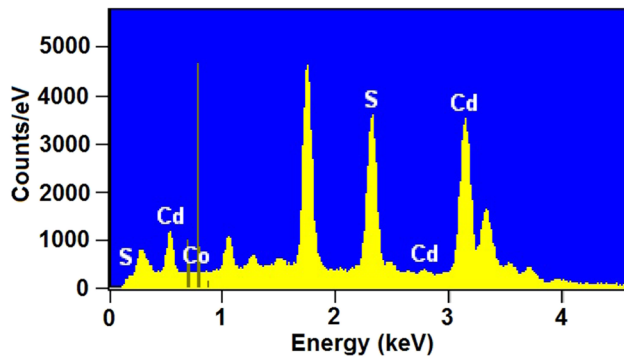


Fig. 1 It is shown a typical EDS spectrum of sample M2, which clearly shows the presence of cobalt. This EDS spectrum was obtained in an area of $10\ \mu\text{m} \times 10\ \mu\text{m}$

and mass percentages of the elements. From these results is observed that Co-doped CdS samples are not stoichiometric. The atomic weight of the ideal unit cell is $\sim 288.95\ \mu$ that corresponds to 22.19% sulphur atoms and 77.81% cadmium atoms as is known. The results presented in Table 1 show that the nanofilms synthesised are not stoichiometric, which contain a low concentration of sulphur, which indicates that they have a high concentration of sulphur vacancies. In addition, it could be induced that there is a high concentration of cadmium and cobalt interstices and/or antisites [15]. Therefore, it can be concluded that if in the synthesised samples there is excess or lack of any constituent chemical element, there would be interstices, antisites or vacancies of them [20].

Figure 2 shows X-ray diffractograms of $\text{Cd}_{1-x}\text{Co}_x\text{S}$ nanofilms with three different cobalt molar concentrations synthesised at $60 \pm 2\ ^\circ\text{C}$. It is observed from X-ray diffraction patterns that deposited CdCoS nanofilms are in polycrystalline nature. The diffraction pattern of the single CdS nanofilms shows clearly a dominant peak at $2\theta = 26.76^\circ$ assigned to (111) plane of ZB CdS crystalline phase, which indicates a preferential growth orientation. Besides, three small peaks at 44.10° , 48.11° and 52.41° that are associated at ZB (220), WZ (103) and ZB (311) diffraction planes of CdS. It observes that each peak corresponds fairly well with data of CdS marked in the software DICVOL04 data. Additionally, two weak peaks are observed on both sides

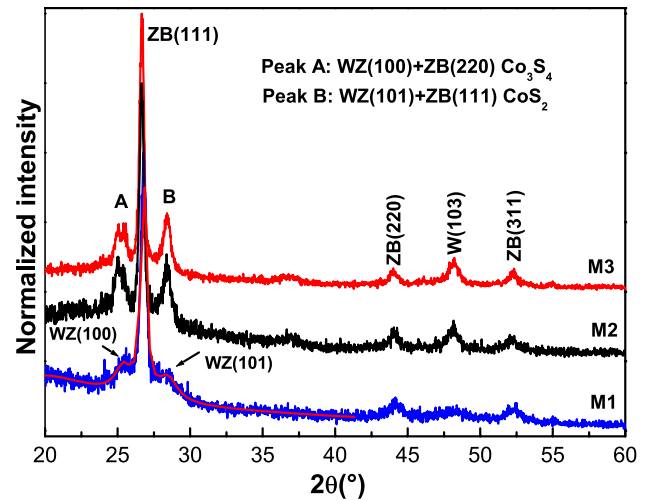


Fig. 2 It presents the X-ray patterns of the three synthesised samples, in which the zinc blende crystalline phase is clearly shown. In addition, the diffraction peaks associated with cobalt are observed for doped samples M2 and M3

of the dominant peak at 26.39° and 28.46° corresponding to the diffraction planes WZ(100) and WZ(101) of CdS, according to the JCPDS-ICDD card No. 10-454. The lattice constant and interplanar distance (ID) obtained with the software DICVOL04 data is in good agreement with the published results [21, 22], whose obtained value is $a = 5.76\ \text{\AA}$ confirmed that the single CBD-CdS nanofilms belong to face-centered cubic system and its X-ray pattern is described in the $Fm-3m(225)$. In the Co-doped CdS diffractograms appear new diffraction peaks that are associated to the incorporation of cobalt at the sub-lattices sites of Cd^{2+} . As is clearly seen in Fig. 2b, c the Co-doped CdS diffractograms present two new diffraction peaks at 17.26° and 26.76° , first one is associated to ZB (220) diffraction plane of Co_3S_4 and the second is assigned to (111) plane of ZB CoS_2 crystalline phase obtained with the software JCPDS-ICDD©2000 data [23]. From X-ray diffraction study can infer that the formation of the CdCoS occurs in the early stage of the films growth, following by the formation of CoS_2 and Co_3S_4 nanocrystallites [24]. In this study has been found that the chemical reaction leads to formation of CdS:CoS nanofilms together with a slight decrease in the

Table 1 It presents the average molar and mass concentrations of Cd, S and Co contained in the nanofilms that were estimated by EDS

Sample	$\text{Co}(\text{NO}_3)_3$ added volume (ml)	Cd mass weight (%)	Cd molar fraction (%)	S mass fraction (%)	S molar fraction (%)	Co mass fraction (%)	Co molar fraction (%)
M1	–	79.20	52.06	20.80	47.94	–	–
	$\text{Co}(\text{NO}_3)_3$					Co	Co
M2	0.5	78.68	52.37	19.33	45.11	1.99	2.52
M3	1.0	75.64	49.11	19.94	45.40	4.42	5.47

nanocrystal size. In addition, it observed a widening in the diffraction peak of the preferential ZB (111) direction, which can be caused by fluctuations in the chemical composition and/or the size of small crystalline domain. Since the used substrates are corning glass, they cannot stress and do not produce mismatch in the lattice constant of the nanolayers. Consequently, the widening of the diffraction peak occurs due to the crystals nanometric size and by presence of strains and crystalline defects that possess multiple facet diffraction peaks, which are the result of NCs polycrystalline growth. In addition, they make the X-ray diffraction peaks do not coincide exactly with the reported plane spacing for ZB phase. Using the Debye–Scherrer equation the nanocrystals sizes were estimated from the widening of the X-ray diffraction peak of the dominant direction ZB (111) [25], which are shown in Table 2, where clearly is observed the Co^{2+} ions effect to replace Cd^{2+} ions of the Cd sub-lattice. The (111) interplanar distance (ID) of the nanofilm ZB crystalline phase was calculated from the 2θ peak position versus Co molar fraction, which increases slightly, see Table 2, that coincides with (111) ID of the bulk CdS ZB crystalline phase. The (111) ID of ZB cubic phase of bulk CdS is 0.3367 nm, which is light lower than the ID values found for the CdS–CdS:Co nanofilms in this work. It is probable that ID values in CdS:Co $^{2+}$ nanofilms are owing to the existence of Cd^{2+} vacancies and probably to all of the possible Co^{2+} species present in Cd^{2+} sites and interstitial positions [20, 26]. Moreover, to the existence of Co_3S_4 and CoS_2 that distort the crystalline lattice and provoke disorder and crystalline defects, which produce a strong strain that affects the interatomic distances [21, 27]. The values of electronegativity for Co (1.88) and Cd (1.69) are favourable to form a solid solution and allow to deposit the nanofilms [28]. It can be seen in Table 2 the CdCoS NCs size slightly decreases as Co molar fraction is increased, suggesting the formation of a solid solution as has been reported [28]. On the other hand, the lattice constant increases lightly as increasing as cobalt concentration is increased in nanolayers, which is an effect of Co^{2+} substituting Cd^{2+} in CdS lattice. A possible explication to this fact can be due to difference of the ionic radii of Cd^{2+} and Co^{2+} , 0.97 and 0.70 Å, respectively.

Figure 3 illustrates the TEM micrographs of two typical samples, in which the presence of particles with an almost

spherical shape at the nanoscale is evident. Based on the measurements taken in the TEM micrographs of the sample size distribution histograms were obtained, which are shown in the insets, and from them can be detected a Gaussian fit with a narrow size distribution and maximum average values of 5.44 and 3.55 nm. As can be seen in Table 2, the NCs size values obtained by the Debye–Scherrer and the Wang equations and those measured from the TEM micrographs have slight discrepancy. These discrepancies in CdCoS NCs sizes are associated to some approximations involved in obtaining the Debye–Scherrer and Wang equations or/and to the coalescence of nanocrystals during the preparation of the samples for TEM analysis, this effect has also been reported for other materials [29]. In order to verify the quality of the structure and the crystalline phase of the obtained semiconductor nanocrystals, HRTEM images were taken and the results are included in Fig. 3. From the HRTEM micrographs, the formation of nanocrystals with a defined crystal structure, zinc blende type, is clearly observed. By amplifying and analysing the selected area of the HRTEM micrographs, it was possible to measure the interplanar distance of 0.33 nm corresponding to the plane (111) of CdS NCs crystallized in the crystalline phase of the zinc-blende type. As can be seen in Table 2, the results obtained by are in good agreement with the results calculated from X-ray diffraction and by Wang equation [29], which will be discussed widely later.

Figure 4 illustrates the Raman spectra of the three nanofilms. Each of the phonon wavenumbers was extracted by fitting the Raman spectrum to a Lorentz line shape. The 1LO and 2LO phonons and multiphonon processes can be clearly observed, which confirm that crystalline phase correspond to a zinc blende (ZB) type. Raman scattering shows that the lattice dynamics is characteristic of bimodal behaviour and the multiphases adjust of the first optical longitudinal mode for the Co-doped CdS denotes the Raman shift of the characteristic peak in the range of 301.4–303.9 cm^{-1} of the CdS crystals, which is associated with the cobalt ions incorporation. In Fig. 5 Raman spectra of two samples are displayed and deconvoluted by Lorentz line shapes. The Raman shift of sample M1 (CdS NCs) appears at $\sim 301.4 \text{ cm}^{-1}$ that is attributed to the longitudinal optical phonon ($A_1(\text{LO})$) mode with a full width at half

Table 2 Mean NCs size of the nanofilms obtained by the Debye–Scherrer equation for the ZB (111) preferred direction and with Wang equation, which show their dependence on the cobalt molar fraction

Sample	a by X-ray (Å)	$d_{(111)}$ by X-ray (nm)	NCs size by X-ray (nm)	NCs size by TEM (nm)	$d_{(111)}$ by HRTEM (nm)	NCs size by Wang equation (nm)
M1	5.76	0.333	2.56	5.44	0.290	1.69
M2	5.79	0.334	1.81	3.42	0.330	1.50
M3	5.78	0.334	1.67	3.39	0.331	1.47

Besides, it presents the grain size obtained by TEM. Additionally, the interplanar distances estimated by X-ray diffraction and by HRTEM are shown

Fig. 3 HRTEM micrographs of the typical synthesised CdS samples are shown: M1 and M2. Additionally, the insets show the histograms that allow to estimate the nanocrystal size

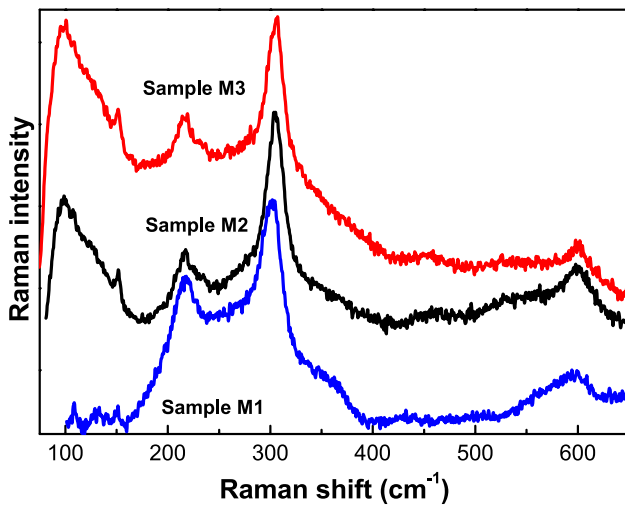
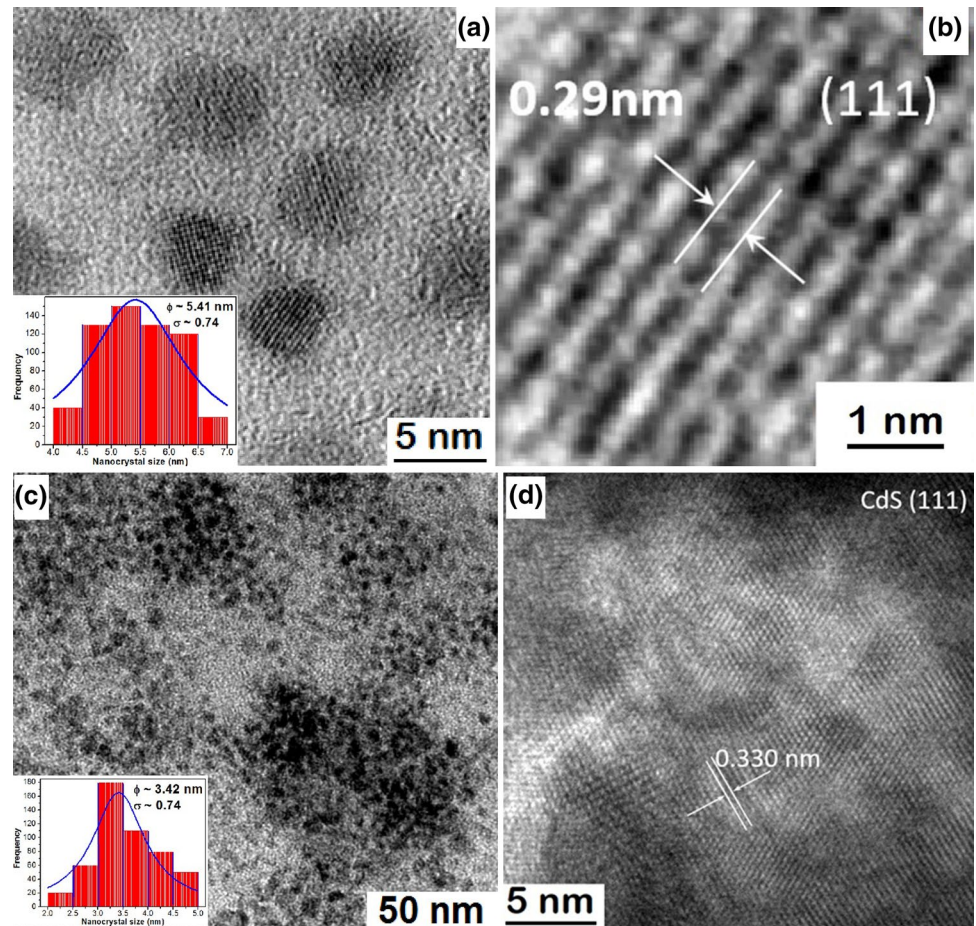


Fig. 4 It shows the Room temperature Raman spectra of the three synthesised CdS nanofilms, undoped and doped ones

maximum (FWHM) of ca. 20.8 cm^{-1} . The 1LO Raman shift of sample M2 (CdCoS NCs) appears at $\sim 303.9 \text{ cm}^{-1}$ with a FWHM of ca. 20.6 cm^{-1} . Finally, the 1LO Raman

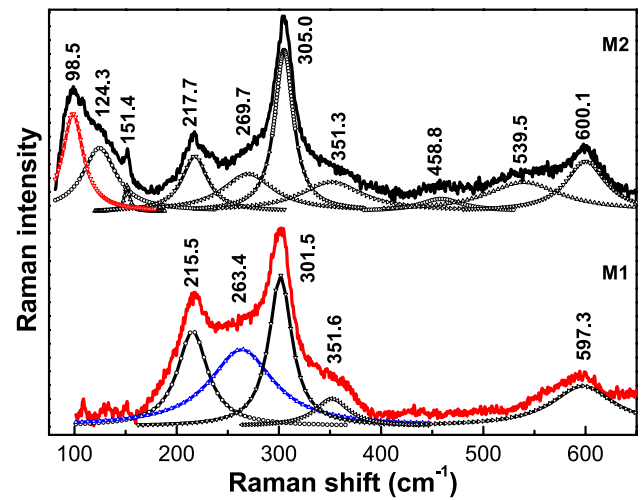


Fig. 5 Deconvolution of the Raman spectra for two samples by Lorentz line shapes: M1 and M2. The -o- lines are their respective fitting

shift of sample M3 (NCs) appears at $\sim 303.8 \text{ cm}^{-1}$ with FWHM of ca. 20.8 cm^{-1} , which indicate that synthesized nanofilms contain a high density of crystalline defects,

since for a nanocrystals free of defects the FWHM should be of the order of ca. 8.0 cm^{-1} [30]. As is observed of these results, the $A_1(\text{LO})$ mode shifts slightly to blue when the cobalt is incorporated. Additionally, the slight decrease of the FWHM of the CdCoS Raman spectrum can be attributed to a slight improvement of the crystallinity of the CdS NCs due to the incorporation of cobalt to Cd sub-lattice. For M1, in addition, to the 1LO phonon and its phononic replica, three vibrational bands are observed at 215.6 , 262.8 and 351.3 cm^{-1} , which are assigned to multiphonon scattering that is consistent with reported elsewhere [20, 31, 32]. The band at 215.6 cm^{-1} can be assigned to multiphonon scattering [25, 26]. The weak band at 351.3 cm^{-1} is the result from the participation of acoustic phonons to the scattering process and the mode corresponding to the low-energy shoulder originates from surface optical phonon modes (SO) at 262.8 cm^{-1} [33, 34] that can be assigned to E_2^H [35]. As is observed in Fig. 5, the frequencies of the vibrational bands slight increase as the Co molar fraction increases, this is consistent because of the cobalt ionic radius is lower than that of cadmium. Additionally, the Raman spectra of CdCoS nanofilms present three vibration modes at 151 , 124 and 98 cm^{-1} well-resolved that can be associated to the combination of longitudinal and transverse acoustic phonon modes in CoS nanocrystals [36], which depend strongly on the molar fraction of incorporated cobalt. The vibration modes are similar to those obtained by the Raman theories and are in accordance with the results of Wijs et al. [37]. It is observed that these bands had a slight blue shift.

The optical properties cobalt doped CdS nanofilms were investigated by room temperature transmittance as function cobalt molar fraction, which were recorded for the nanofilms in the wavelength range, $300\text{--}900 \text{ nm}$. The sharp reduction in the transmittance spectra at the wavelengths close to 300 nm is due to the fundamental absorption edge of the nanofilm. The main edge band blue shifts as $V[\text{Co}^{2+}]$ increases compared to the single CdS that is indicative that the cobalt atoms are being incorporated into interstitial cell unit, which reduces the NCs size, see Table 2. As is known the optical band gap (E_g) energy of a semiconductor is related to the optical absorption coefficient (α) and to the incident photon energy ($h\nu$). The absorption coefficient (α) for a film of thickness d and reflectance R is determined near the absorption edge by using the relation:

$$\alpha = \ln \left\{ (1 - R)^2 / T + \left[((1 - R)^2 / 2T)^2 + R^2 \right]^{1/2} \right\} / d$$

The CdS:Co²⁺ optical band gap energy has been evaluated from the transmittance spectrum using the Tauc relation [38–41]: $ah\nu = (E_G - h\nu)^n$, where n depends on the kind of optical transition that prevails. Specifically, n is $1/2$ and

2 when the transition is direct and indirectly allowed. The CdS is a semiconductor compound with a direct allowed transition. The CdCoS band gap energy was estimated from the linear portion of the graph $(ah\nu)^2$ vs. $h\nu$ as is illustrated in Fig. 6, the obtained results are shown in Table 2. The optical band gap energy estimated of the single CdS nanofilm (M1 sample) is of 2.56 eV that is 138 meV higher than optical band gap energy of bulk CdS, which is indicative that there is a high quantum-confinement associated to the NCs average grain size [42, 43]. As is observed in Fig. 6b band gap energy blue shifts with the $V[\text{Co}^{2+}]$ increase, this increase can be explained due to the substitution in the lattice of cadmium atoms (ionic radii $\sim 0.95 \text{ \AA}$) by cobalt atoms (ionic radii 0.70 \AA) that is clearly smaller. It is observed that the band gap energies of the semiconductor nanocrystals were higher than the value of bulk CdS at room temperature (2.42 eV). The optical cut-off energy shows a blue shift from 0.138 to 1.383 eV , which

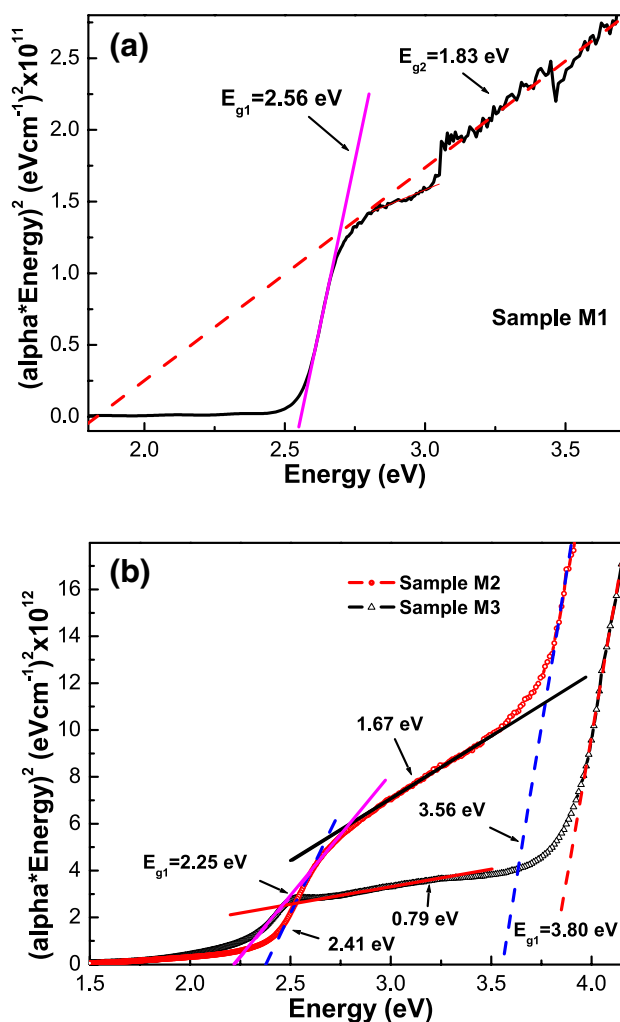


Fig. 6 Tauc plots to calculate the band gap energy for the synthesised CdS nanofilms: **a** CdS and **b** Co-doped CdS

confirms the formation of CdS nanocrystals. The optical band gap energy of the M3 sample is of 3.803 eV [44], this value is the highest of the synthesised samples and can be associated to that the nanocrystals size is smaller than Bohr's excitonic radius, 1.88 nm. Widening of band gap with the incorporation of Co can be attributed to the sp–d exchange interactions between the band electrons in CdS and the localized d electrons of the Co^{2+} [45, 46]. As the band gap energy increases, it means that the nanocrystal size decreases. In order to determine the average particle size of $\text{Cd}_{1-x}\text{Co}_x\text{S}$ NCs the Wang equation was also used [47, 48]:

$$E_{GNP} = E_{Gbulk} + \frac{\hbar^2 \pi^2}{2r^2 \mu^*} - \frac{1.786e^2}{\epsilon_r \epsilon_0 r}$$

where E_{GNC} is the energy of band gap of the NCs CdS estimated by transmittance previously, E_{Gbulk} is the band gap energy of bulk CdS, $r = d_{ab}/2$, d_{ab} is the diameter of the nanocrystals, and ϵ_r is the permittivity of nano CdS and the rest of the parameters have already been defined elsewhere. The effective mass μ^* is defined as $1/\mu^* = 1/2(1/m_e^* + 1/m_h^*)$. For CdS $m_e^* = 0.19m_0$ and $m_h^* = 0.8m_0$ and $\epsilon_r = 5.7$ is the CdS dielectric constant. The estimated NCs sizes are presented in Table 2, which are smaller than Bohr's excitonic radius of the CdS and are of the same order as the crystal sizes estimated by X-ray diffraction.

Figure 7 shows the photoluminescence spectra of the single and doped CdS nanofilms. Figure 7a shows the photoluminescence spectrum deconvolution of sample M1, which presents radiative transitions at 2.86, 2.37, 2.19, 1.88 and 1.38 eV. The main radiative band at 2.86 eV (violet band) is associated a radiative transition band-to-band, which is higher than the undoped CdS band gap energy for 302 meV. That is due to the quantum-confinement associated with nanometric grain size since it is less than the Bohr excitonic radius. The green band at 2.37 eV is called the optical signature of interstitial oxygen [49]. The green-yellow band at 2.19 eV could be attributed to the CdO complexes that would form during the growth process due to the presence of oxygen during the nucleation of the nanofilm, since the CdO band gap energy is about 2.16 eV [50]. The broad band observed at 1.88 eV (orange–red band), which is named the “orange band”, it has been observed between 2.03 and 2.08 eV depending of the growth technique [51, 52], it is associated to a donor–acceptor pair (DAP) radiative transition between a donor level and an unidentified acceptor level. The ionization energy of this donor level has estimated to be between 120 and 260 meV, which corresponds to interstitial cadmium ($I_{Cd^{2+}}$) [49]. Finally, the broad and weak peak observed at 1.38 eV, it is in the infrared region

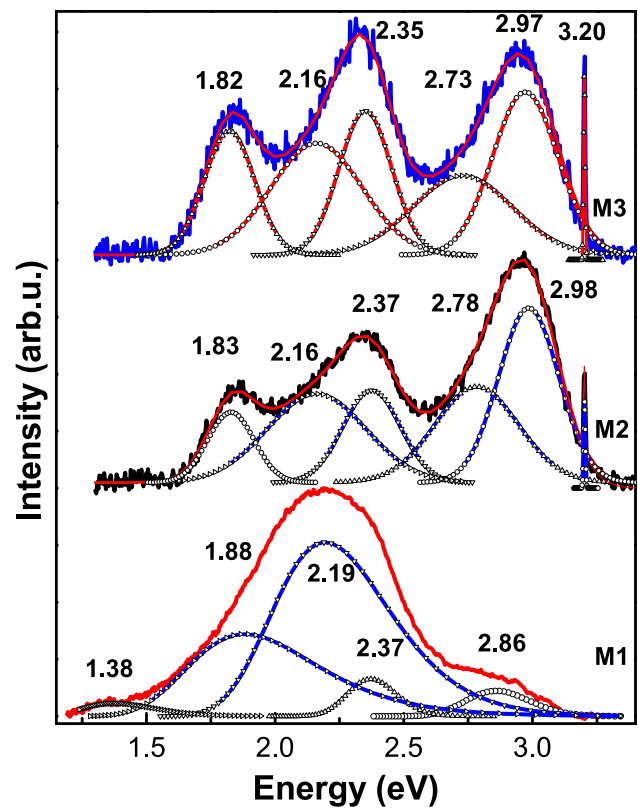


Fig. 7 It illustrates the room temperature photoluminescence and their deconvolution of three synthesised samples, undoped and doped ones

and is associated with unidentified deep impurities. Figure 7b, c illustrates the two photoluminescence spectra of the Co-doped CdS samples, which clearly the effect of the cobalt incorporation in the cadmium sub-lattice is observed. CdS:Co²⁺ PL spectra present six radiative transitions about 3.20, 2.97, 2.73, 2.37, 2.16 and 1.83 eV. The last three radiative transitions have the same origin discussed previously for undoped CdS nanofilms. It is clearly observed in the Co-doped CdS PL spectra the green band at 2.37 eV, which is called the optical signature of interstitial oxygen, has increased its intensity. Being the dominant band for photoluminescence of the sample M3, which is due to the transition of electrons from defect donor levels to the valance band/midgap states [7, 53] and possibly to contributions of oxygen interstices [49]. The blue band at 2.73 eV was associated with the emission due to electronic transition from the conduction band to an acceptor level due to Co [54]. The emission peaks at 2.98 (violet band) and 3.20 eV (ultraviolet band) are usually observed from the excitonic emission luminescence due to the quantum confinement.

5 Conclusions

In this work reported the growth successfully of Co-doped CdS nanostructures synthesised by chemical bath deposition technique at 60 ± 2 °C. The crystalline structure of the nanostructures was zinc blende type in the (111) direction, which was obtained by X-ray diffraction and Raman spectroscopy. The incorporation of cobalt in the CdS lattice was confirmed by EDS and X-ray diffraction. The nanocrystal size was determined by the Debye–Scherrer equation from ZB (111) direction, by the Wang equation and TEM, which was 2.56 nm for the CdS and 1.81–1.67 nm for Co-doped CdS that were confirmed by TEM. As was discussed, the NCs size values obtained by the Debye–Scherrer, the Wang equations and those measured from the TEM micrographs had slight discrepancy. These discrepancies in CoCdS NCs sizes were associated to some approximations involved in obtaining the Debye–Scherrer and Wang equations or/and to the coalescence of nanocrystals during the preparation of the samples for TEM analysis. These NCs sizes confirmed the quantisation effect in the synthesised samples due to are lower than the exciton Bohr radius. The Co-doped CdS exhibited a direct band gap that slightly increases with increase of the Co molar fraction, from 2.56 to 3.80 eV, in the investigated range that was obtained by transmittance measurements. The room temperature photoluminescence of the undoped CdS presents the band–band transition associated to CdS nanocrystals size and the radiative transitions associated with residual impurities and structural defects, mainly the optical signature of interstitial oxygen. For the Co-doped CdS, the photoluminescence presents, in addition to the radiative transitions previously discussed for the CdS, an excitonic transition at 3.20 eV was observed.

References

1. Q. Cao, M. Fu, G. Liu, H. Zhang, S. Yan, Y. Chen, L. Mei, J. Jiao, *J. Appl. Phys.* **115**, 243906 (2014)
2. T. Shi, S. Zhu, Z. Sun, S. Wei, W. Liu, *Appl. Phys. Lett.* **90**, 102108 (2007)
3. S.W. Lim, D.K. Hwang, J.M. Myoung, *Solid State Commun.* **125**, 231 (2003)
4. J.H. Kim, H. Kim, D. Kim, Y.E. Ihm, W.K. Choo, *Phys. B* **327**, 304 (2002)
5. J.H. Kim, H. Kim, D. Kim, Y.E. Ihm, W.K. Choo, *J. Eur. Ceram. Soc.* **24**, 1847 (2004)
6. M.A. Baghchesara, M. Cheraghizade, F. Jamali-Sheini, R. Yousefi, *J. Mater. Sci.: Mater. Electron.* **28**, 4475–4480 (2017)
7. L. Saravanan, A. Pandurangan, R. Jayavel, *J. Nanopart. Res.* **13**, 1621 (2011)
8. R.N. Bhargava, D. Gallagher, X. Hong, A. Nurmikko, *Phys. Rev. Lett.* **72**, 416 (1994)
9. J.K. Furdyna, N. Samarth, *J. Appl. Phys.* **61**, 3526 (1987)
10. S.M. Uba, J.M. Baranowski, *Phys. Rev. B* **17**, 69 (1978)
11. Z. Mierczyk, A. Majchrowski, K. Ożga, A. Slezak, I.V. Kityk, *Opt. Laser Technol.* **38**, 558 (2006)
12. M.A. Baghchesara, R. Tousefi, M. Cheraghizade, F. Jamali-Sheini, A. Sa’edi, *Ceram. Int.* **42**, 1891 (2016)
13. R. Yousefi, J. Beheshtian, S.M. Seyed-Talebi, H.R. Azimi, F. Jamali-Sheini, *Chem. Asian J.* (2017). <https://doi.org/10.1002/asia.201701423>
14. Q.Q. Liu, J.H. Shi, Z.Q. Li, D.W. Zhang, X.D. Li, Z. Sun, L.Y. Zhang, S.M. Huang, *Phys. B* **405**, 4360 (2010)
15. D. Albin, D. Rose, R. Dhere, D. Levi, L. Woods, A. Swartzlander, P. Sheldon, 26th IEEE Photovoltaic Specialists Conf. 1977, Anaheim CA, NREL/CP 520-22949
16. C.M. Dai, L. Horng, W.F. Hsieh, Y.T. Shih, C.T. Tsai, D.S. Chuu, *J. Vac. Sci. Technol. A* **10**, 484 (1992)
17. H.M. Upadhyaya, S. Chandra, *J. Mater. Sci.* **29**, 2734 (1994)
18. S. Radhu, C. Vijayan, *Mater. Chem. Phys.* **129**, 1132 (2011)
19. W.Q. Peng, G.W. Cong, S.C. Qu, Z.G. Wang, *Nanotechnology* **16**, 1469 (2005)
20. J. Díaz-Reyes, J.I. Contreras-Rascón, M. Galván-Arellano, J.S. Arias-Cerón, J.E.M. Gutiérrez-Arias, J.E. Flores-Mena, M.M. Morín-Castillo, *Braz. J. Phys.* **46**, 612 (2016)
21. J. Singh, *Physics of Semiconductors and their Heterostructures* (Mc Graw-Hill, New York, 1993)
22. K. Yamaguchi, T. Yoshida, T. Sugiura, H. Minoura, *J. Phys. Chem. B* **102**, 9677 (1998)
23. J.L. Pratt, P. Bayliss, *Zeitschrift für Kristallographie* **150**, 163 (1979)
24. M. Guglielmi, A. Martucci, J. Fick, G. Vitrant, *J. Sol-Gel. Sci. Technol.* **11**, 229 (1998)
25. J.A. Lange’s, *Handbook of Chemistry* (McGraw Hill Book Co., Beijing, 1999)
26. M. Grus, A. Sikorska, *Phys. B* **266**, 139 (1999)
27. J. Díaz-Reyes, J.I. Contreras-Rascón, J.S. Arias-Cerón, J.F. Sánchez-Ramírez, M. Galván-Arellano, J. Martínez-Juárez, J.A. Balderas-López, *Mat. Sci. Semicond. Proc.* **37**, 199 (2015)
28. J.A. Dean, *Lange’s Handbook of Chemistry*, 13th edn. (McGraw-Hill, New York, 1987)
29. F. Ángel-Huerta, M.P. González-Araoz, J.F. Sánchez-Ramírez, J. Díaz-Reyes, J.L. Herrera-Pérez, J.S. Arias-Cerón, J.G. Mendoza-Álvarez, *J. Lumin.* **197**, 277 (2018)
30. M. Froment, M.C. Bernard, R. Cortes, B. Mokili, D. Lincot, *J. Electrochem. Soc.* **142**, 2642 (1995)
31. S. Kar, B. Satpati, P.V. Satyam, S. Chaudhuri, *J. Phys. Chem. B* **109**, 19134 (2005)
32. C. Hu, X. Zeng, J. Cui, H. Chen, J. Lu, *J. Phys. Chem. C* **117**, 20998 (2013)
33. F. Comas, N. Studart, G.E. Marques, *Solid State Commun.* **130**, 477 (2004)
34. H. Lange, M. Artemyev, U. Woggon, C. Thomsen, *Phys. Status Solidi (b)* **246**, 2817 (2009)
35. H.M. Fan, Z.H. Ni, Y.P. Feng, *Appl. Phys. Lett.* **91**, 171911 (2007)
36. G.D. Smith, S. Firth, R.J.H. Clark, M. Cardona, *J. Appl. Phys.* **92**, 4375 (2002)
37. G.A. de Wijs, R.A. de Groot, *Acta* **46**, 1989 (2001)
38. J.I. Contreras-Rascón, J. Díaz-Reyes, J.E. Flores-Mena, M. Galván-Arellano, L.A. Juárez-Moran, R.S. Castillo-Ojeda, *Curr. Appl. Phys.* **15**, 1568 (2015)
39. M.R. Loghman-Estarki, M. Hajizadeh-Oghaz, H. Edris, R.S. Razavi, *CrystEngComm.* **15**, 5898 (2013)
40. D.J. Seo, *J. Korean Phys. Soc.* **45**, 1575 (2004)
41. B.J. Jin, H.S. Woo, S. Im, S.H. Bae, S.Y. Lee, *Appl. Surf. Sci.* **169/170**, 521 (2001)
42. J.L. Pankove, *Optical Processes in Semiconductors* (Prentice-Hall, Englewood Cliffs, NJ, 1971)
43. F. Gao, Y. Wang, L. Zhang, W. Yang, L. An, *J. Am. Ceram. Soc.* **93**, 1364 (2010)

44. G. Giribabu, G. Murali, D.Amaranatha Reddy, C. Liu, R.P. Vijayalakshmi, *J. Alloys Compd.* **581**, 363 (2013)
45. E. Bacaksiz, M. Tomakin, M. Altunbas, M. Parlak, T. Colakoglu, *Phys. B* **403**, 3740 (2008)
46. P. Koidl, *Phys. Rev. B* **15**, 2493 (1977)
47. A.D. Yoffe, *Adv. Phys.* **42**, 173 (1993)
48. Y. Wang, A. Suna, W. Mahler, R. Kasowski, *J. Chem. Phys.* **87**, 7315 (1987)
49. F. Gemain, I.-C. Robin, S. Renet, S. Bernardi, *Phys. Status Solidi C* **9**, 1740 (2012)
50. P.H. Jefferson, S.A. Hatfield, T.D. Veal, P.D.C. King, C.F. McConville, J. Zúñiga-Pérez, V. Muñoz-Sanjosé, *Appl. Phys. Lett.* **92**, 022101 (2008)
51. K. Mochizuki, M. Satoh, K. Igaki, *Jpn. J. Appl. Phys.* **22**, 1414 (1983)
52. A.E. Abken, D.P. Halliday, K. Durose, *J. Appl. Phys.* **105**, 064515 (2009)
53. H. Cao, G. Wang, S. Zhang, X. Zhang, D. Rabinovich, *Inorg. Chem.* **45**, 5103 (2006)
54. T. Lavanya, K. Satheesh, N.V. Jaya, *IOP Conf. Ser. Mater. Sci. Eng.* **73**, 012114 (2015)